*fractal and fractional*

MDPI

*Article*

# A New Approach Based on Metaheuristic Optimization Using Chaotic Functional Connectivity Matrices and Fractal Dimension Analysis for AI-Driven Detection of Orthodontic Growth and Development Stage

**Orhan Cicek [1], Yusuf Bahri Özçelik [2] and Aytaç Altan [2,*]**

[1] Department of Orthodontics, Faculty of Dentistry, Zonguldak Bülent Ecevit University, Zonguldak 67600, Turkey; orhancicek@beun.edu.tr
[2] Department of Electrical Electronics Engineering, Zonguldak Bülent Ecevit University, Zonguldak 67100, Turkey; ybahri.ozcelik@beun.edu.tr
* Correspondence: aytacaltan@beun.edu.tr

**Abstract:** Accurate identification of growth and development stages is critical for orthodontic diagnosis, treatment planning, and post-treatment retention. While hand–wrist radiographs are the traditional gold standard, the associated radiation exposure necessitates alternative imaging methods. Lateral cephalometric radiographs, particularly the maturation stages of the second, third, and fourth cervical vertebrae (C2, C3, and C4), have emerged as a promising alternative. However, the nonlinear dynamics of these images pose significant challenges for reliable detection. This study presents a novel approach that integrates chaotic functional connectivity (FC) matrices and fractal dimension analysis to address these challenges. The fractal dimensions of C2, C3, and C4 vertebrae were calculated from 945 lateral cephalometric radiographs using three methods: fast Fourier transform (FFT), box counting, and a pre-processed FFT variant. These results were used to construct chaotic FC matrices based on correlations between the calculated fractal dimensions. To effectively model the nonlinear dynamics, chaotic maps were generated, representing a significant advance over traditional methods. Feature selection was performed using a wrapper-based approach combining k-nearest neighbors (kNN) and the Puma optimization algorithm, which efficiently handles the chaotic and computationally complex nature of cervical vertebrae images. This selection minimized the number of features while maintaining high classification performance. The resulting AI-driven model was validated with 10-fold cross-validation and demonstrated high accuracy in identifying growth stages. Our results highlight the effectiveness of integrating chaotic FC matrices and AI in orthodontic practice. The proposed model, with its low computational complexity, successfully handles the nonlinear dynamics in C2, C3, and C4 vertebral images, enabling accurate detection of growth and developmental stages. This work represents a significant step in the detection of growth and development stages and provides a practical and effective solution for future orthodontic diagnosis.

**Keywords:** cervical vertebrae; growth and development; chaotic and fractal functional connectivity matrices; fractal dimension analysis; artificial intelligence; metaheuristic Puma optimizer algorithm

check for updates

Academic Editor: Yifei Pu

Received: 25 January 2025
Revised: 12 February 2025
Accepted: 21 February 2025
Published: 26 February 2025

**Citation:** Cicek, O.; Özçelik, Y.B.; Altan, A. A New Approach Based on Metaheuristic Optimization Using Chaotic Functional Connectivity Matrices and Fractal Dimension Analysis for AI-Driven Detection of Orthodontic Growth and Development Stage. *Fractal Fract.* **2025**, *9*, 148. https://doi.org/10.3390/fractalfract9030148

**Copyright:** © 2025 by the authors. Licensee MDPI, Basel, Switzerland. This article is an open access article distributed under the terms and conditions of the Creative Commons Attribution (CC BY) license (https://creativecommons.org/licenses/by/4.0/).

## 1. Introduction

Orthodontics plays a pivotal role in improving not only dental aesthetics but also overall oral health and functionality. Accurate determination of skeletal maturation is a cornerstone of orthodontic diagnosis and treatment planning. This knowledge is essential to guide orthodontists in timing interventions, predicting growth patterns, and achieving long-term treatment stability [1]. Successful orthodontic outcomes are highly dependent on understanding the developmental stages of the patient's skeletal system, which significantly influences the timing and approach of treatment strategies [2].

Among the methods available to assess skeletal maturation, radiographic assessment remains indispensable. This approach has evolved over time to strike a balance between diagnostic accuracy and patient safety. Especially in the growth modification procedures used in functional orthopedics, accurate assessment of growth and developmental stages is essential to optimize treatment planning. Traditionally, hand–wrist radiographs have been used to assess skeletal maturation, providing a reliable criterion for determining the timing of growth spurts. However, the challenges posed by the additional radiation exposure required for these radiographs and the need for experience in visual assessment for an accurate diagnosis have prompted the search for alternative approaches. In this context, cervical vertebrae maturation (CVM) stages derived from lateral cephalometric radiographs have emerged as a viable, radiation-free, and easily applicable method for routine clinical practice [3,4].

Hand and wrist radiographs have long been considered the gold standard for determining skeletal maturation. These radiographs provide detailed information on the developmental status of the hand and wrist bones, allowing clinicians to identify critical growth stages [5]. However, concerns about cumulative radiation exposure, particularly in younger patients undergoing multiple radiographic imaging sessions, have led to interest in alternative methods. The morphologic analysis of the cervical vertebrae visible in lateral cephalometric radiographs offers an attractive solution by allowing the evaluation of skeletal maturation. This technique focuses on the visual assessment of morphological changes in the shape of each cervical vertebrae, second (C2), third (C3), and fourth (C4), as reliable indicators of growth and developmental stages. By utilizing radiographs already used in routine orthodontic evaluations, the CVM method minimizes additional radiation exposure while maintaining diagnostic accuracy [6,7].

In addition to the advantages and challenges mentioned above, the intricate structure of these cervical vertebrae exhibits fractal geometry, which is characterized by self-similarity and complexity across scales. This fractal nature reflects the non-linear developmental processes that underpin skeletal growth and presents difficulties for conventional imaging analysis techniques [8]. Traditional approaches often struggle to capture and interpret the complexity inherent in vertebral morphology, necessitating the use of advanced computational methods capable of modeling these non-linear dynamics. As a result, there is an increasing need for quantitative and objective methods to improve the accuracy and reliability of skeletal maturation assessments [9,10].

Fractal analysis has emerged as a promising quantitative approach to characterizing the irregularities inherent in vertebral morphology. By calculating fractal dimensions, researchers can quantify the degree of structural complexity and irregularity in cervical vertebrae images. Fractal dimensions provide a robust measure of morphological complexity, allowing a deeper understanding of the developmental processes that shape skeletal structures [11]. However, these methods need to be complemented by robust frameworks to deal with the chaotic dynamics often associated with growth and development. Advances in artificial intelligence (AI) and machine learning have opened new avenues for integrating

fractal analysis with computational models, offering the potential for more accurate and efficient diagnostic tools [12,13].

In recent years, AI and deep learning (DL)-based methods have achieved remarkable progress in medical imaging, particularly in tasks requiring automatic classification and segmentation [14,15]. DL models have demonstrated the ability to minimize observer-dependent variations commonly encountered in manual and visual assessments, providing more consistent and rapid results. These technologies hold considerable potential for evaluating skeletal maturation and growth stages in complex processes, such as cervical vertebrae analysis. By automating the analysis of CVM stages, AI-based tools can reduce diagnostic variability and improve clinical decision-making [16,17].

The motivation for this paper is to address the critical need for accurate and objective methods that minimize chair time and eliminate radiation exposure in the assessment of skeletal maturation in orthodontic practice. Existing techniques, such as hand–wrist radiographs, although effective, involve additional radiation exposure and are subject to observer variability in manual and visual assessment. This study aims to utilize lateral cephalometric radiographs and integrate advanced computational techniques, including fractal dimension analysis and AI, to provide a more reliable and safer alternative. By addressing the challenges posed by the fractal and nonlinear nature of cervical vertebrae morphology, the proposed methodology aims to improve diagnostic accuracy and support personalized orthodontic treatment planning. The main contributions of this study are summarized as follows:

- Novel Computational Framework: Introduces an innovative methodology combining fractal dimension analysis with CFC matrices to model the nonlinear and fractal dynamics of cervical vertebrae.
- Advanced Fractal Analysis: Utilizes three distinct methods (fast Fourier transform (FFT), box counting, and a pre-processed FFT variant) to compute robust fractal dimensions of C2, C3, and C4 vertebrae.
- Chaotic Functional Connectivity: Constructs matrices capturing intricate relationships between fractal measures, providing a comprehensive understanding of growth dynamics.
- Integration with AI: Leverages AI and DL techniques to automate cervical vertebrae analysis, reducing observer variability and enhancing diagnostic precision.
- Radiation-Free Alternative: Offers a practical solution using lateral cephalometric radiographs already integrated into routine clinical workflows, minimizing additional radiation exposure.
- Advancing Orthodontic Practice: Provides a scalable and objective framework that supports personalized and effective orthodontic treatment planning following accurate diagnosis by improving the reliability of skeletal maturation assessments.

This study aims to contribute to this evolving field by proposing a novel methodology that combines CFC matrices with fractal dimension analysis to model the nonlinear and fractal dynamics of cervical vertebrae. The fractal dimensions of the C2, C3, and C4 vertebrae were computed using three distinct methods: FFT [18], box counting [19], and a pre-processed FFT variant. These dimensions were then used to construct CFC matrices [20] that capture the intricate relationships between fractal measures. By integrating these advanced computational techniques, the proposed methodology seeks to address the limitations of traditional approaches and provide a more comprehensive framework for assessing skeletal maturity.

The remainder of this paper is organized as follows. Section 2 discusses the background of the study and provides a comprehensive review of related works on the detection of orthodontic growth and development stages, with a particular focus on AI-driven ap-

proaches and fractal dimension analysis. Section 3 elaborates on the proposed methodology, which integrates chaotic and fractal functional connectivity (CFFC) matrices, fractal dimension analysis, and metaheuristic optimization techniques, including the wrapper-based Puma optimization (PO) algorithm, to develop a robust AI-driven detection model. The experimental results are presented in Section 4, along with an in-depth discussion of the model's performance, comparison with existing methods, and clinical implications. Finally, Section 5 summarizes the findings and highlights the conclusions and potential directions for future research.

## 2. Background and Related Works

Understanding growth and development through skeletal maturation is a critical component of orthodontic treatment planning. The CVM method, derived from cephalometric radiographs, has emerged as a reliable approach to assessing skeletal age and predicting pubertal growth spurts. While traditional methods relied on hand–wrist radiographs to determine growth and development stages, CVM analysis integrates seamlessly into routine orthodontic diagnosis, eliminating the need for additional radiation exposure. Chronological age, often used as a baseline indicator, lacks the precision required to reflect individual growth patterns. Instead, skeletal age, as determined by radiographic markers, provides a more accurate framework for identifying optimal treatment periods in orthodontics. Such advances are needed to address the complexities of growth prediction and improve treatment planning outcomes [7,21].

CVM staging is only one aspect of orthodontic assessment and treatment. Orthodontists should comprehensively analyze clinical and radiographic (especially lateral cephalometric) data to arrive at an appropriate diagnosis and treatment plan. Despite specialization, this process requires considerable time and expertise, as well as a high degree of reproducibility. Studies have shown that trained examiners achieve a 98% reproducibility rate when visually classifying CVM stages. Automating this process through AI-driven methods promises to increase accuracy, efficiency, reproducibility, and time savings, thereby improving patient care and treatment planning [2,6,22].

Traditionally, the gold standard for determining skeletal maturation and growth potential has been hand–wrist radiographs, which have long been considered a reliable tool. However, the advent of cephalometric radiography provided an alternative that reduced radiation exposure while providing a comprehensive analysis of skeletal growth. The use of cervical vertebrae to determine skeletal maturation stages has gained widespread acceptance in orthodontics due to its integration into routine diagnostic procedures. Despite this, the implementation of AI in the analysis of cephalometric radiographs remains in its early stages, with limited studies addressing the application of advanced machine learning and DL techniques in this area [7,21,23].

The integration of AI technologies into CVM analysis has revolutionized the field, providing automated, efficient, and highly reproducible methods for assessing skeletal maturation. Amasya et al. [14] investigated various machine learning models, including artificial neural networks (ANNs), support vector machines (SVMs), decision trees (DTs), and random forests (RFs), for CVM classification and identified ANN as the most effective model with a weighted $\kappa = 0.926$. This result highlights the robustness of ANNs in automating CVM analysis, achieving superior accuracy compared to traditional methods. The study highlights how AI can reduce observer variability and streamline orthodontic diagnosis. Building on these findings, Kök et al. [24] developed 24 ANN models to classify growth stages using datasets containing age and 32 linear measurements. The researchers achieved a remarkable accuracy of 94.27%, demonstrating the scalability and precision of ANN-based systems in orthodontics. This study further explored how to optimize the

balance between computational efficiency and diagnostic effectiveness by incorporating fewer linear measurements while maintaining high accuracy. This approach demonstrates the potential for creating clinically applicable AI models that minimize complexity without compromising performance.

Deep learning models have further improved CVM classification through innovative architectural designs and image processing techniques. Atici et al. [25] introduced TriPodNet, a parallel structured neural network designed to automatically classify CVM stages. By processing cephalometric radiographs with edge enhancement filters, the model achieved a classification accuracy of 81.18% for females and 75.32% for males. The study highlighted the importance of pre-processing techniques such as edge enhancement in improving classification accuracy. This highlights the role of image quality and feature extraction in improving model performance. Khazaei et al. [17] used deep convolutional neural networks (CNNs) to classify pubertal growth spurts, achieving 93% accuracy in binary classification and 82% in three-class scenarios. The study used the ConvNeXtBase-296 architecture and applied data augmentation techniques, demonstrating the potential of transfer learning to improve performance even with limited datasets. By focusing on the C2–C4 regions, the research highlights the importance of region of interest (ROI) selection in improving CNN-based models. The results indicate that CNNs are capable of accurately assessing skeletal maturity, even when faced with limited data availability. The impact of ROI selection on classification accuracy is further demonstrated by Kresnadhi et al. [26] who evaluated several deep learning architectures including ResNet101, InceptionV3, and InceptionResNetV2. Their results showed that InceptionResNetV2 achieved the highest accuracy when focusing on cropped C2–C6 regions, demonstrating the importance of targeted image processing. This approach not only improves the accuracy but also overcomes the challenges associated with interpreting multi-scale features. The study illustrates how refining input data and focusing on critical areas can improve model performance and reliability. In another study, Motie et al. [27] developed a multi-stage deep learning framework that combined Faster R-CNN for region detection with ResNet 101 classifiers. This framework classified CVM stages into six classes and achieved an overall accuracy of 82.96%. The modular nature of this framework, which divides tasks into region-specific and stage-specific classifiers, provides a scalable and efficient approach to complex classification tasks. The study highlights the potential of combining region detection and classification to create robust AI systems. AI-driven systems have also been explored for their ability to provide continuous and dynamic assessments of skeletal maturation. Atici et al. [16] developed AggregateNet, a parallel structured DL model that incorporated age and gender information into the classification process. The model processed cephalometric radiographs with edge enhancement filters and achieved accuracies of 82.35% for females and 75% for males. When the edge filters were removed, accuracy decreased, highlighting the critical role of pre-processing in maintaining high performance. The system's integration of multiple input modalities demonstrates the adaptability of AI in creating comprehensive diagnostic tools. Similarly, Li et al. [28] proposed the psc-CVM system, a three-stage DL model consisting of a localization network, a shape recognition network, and a CVM evaluation network. By processing 10.200 lateral cephalograms, the system achieved an area under the curve (AUC) of 0.94, with an overall accuracy of 70.42% on the test set. These results demonstrate the promise of modular architectures in addressing complex classification tasks. The study also highlights the importance of using diverse datasets to ensure model generalizability across different populations.

Despite these advances, challenges remain in the implementation of AI in CVM analysis. Akay et al. [29] reported moderate accuracy (58.66%) in CNN-based CVM classification, highlighting the need for further refinements in data pre-processing and ROI selection.

The study also highlighted the potential for AI systems to improve with larger datasets and more sophisticated architectures. The variability of datasets, the interpretability of AI models, and the need for standardized validation protocols remain significant hurdles. This study is the first attempt to combine advanced techniques such as CFFC matrices with metaheuristic optimization for CVM classification. By addressing both computational complexity and classification accuracy, it aims to bridge the gap between theoretical advances and practical applications in orthodontics. The importance of this research lies in its potential to provide robust and scalable AI-driven tools that significantly improve diagnostic accuracy and efficiency. With this foundation, we now move on to Section 3, where we present new methods for improving CVM classification.

## 3. Framework of the Detection Algorithm for Orthodontic Growth Stages: Integrating Chaotic and Fractal Functional Connectivity Matrices, Fractal Dimension Analysis, and Metaheuristic Optimization

This section presents our proposed framework for detecting orthodontic growth and development stages with a balance between computational efficiency and high classification accuracy. The framework starts with the extraction of fractal dimensional features that capture the geometric complexity in cervical vertebrae images. These features are complemented by CFFC analysis, which models non-linear dynamics and intricate dependencies in the data. To improve feature relevance, a wrapper-based feature selection process is applied using the PO algorithm, which identifies the most significant features while minimizing redundancy. For classification, the selected feature vectors are fed into a k-nearest neighbors (kNNs) classifier, which is optimized to ensure robust and accurate stage predictions. Performance metrics including accuracy (Acc), precision (Prec), recall (Rec), and F1 score (F1-score) are used to comprehensively evaluate the effectiveness of the model. The detailed methodology underlying each step of the orthodontic growth and development stage detection framework is described in the following subsections.

### *3.1. Fractal Dimension Analysis*

Fractal dimension analysis is a powerful tool for quantifying the complexity, self-similarity, and scaling behavior of patterns in datasets or images. The analysis often uses methods such as FFT, box counting, and the pre-processed FFT variant to estimate the fractal dimension. These methods use mathematical formulas to extract structural features that provide insights into the underlying fractal nature. These methods are described in detail below with their respective formulas.

#### 3.1.1. Fast Fourier Transform Method

The FFT method estimates the fractal dimension by analyzing the spatial frequency components of the data. This is achieved by applying a Fourier transform to the dataset or image to compute the power spectrum [18].

Step 1: Compute the Fourier transform $\mathcal{F}(f)$ of the image or data:

$$\mathcal{F}(f) = \int_{-\infty}^{\infty} I(x,y) e^{-2\pi i(fxx+fyy)} dxdy \tag{1}$$

where $I(x,y)$ is the intensity at spatial position $(x,y)$, and $f$ represents spatial frequencies.

Step 2: Calculate the power spectrum:

$$P(f) = |\mathcal{F}(f)|^2 \tag{2}$$

Step 3: Create a log–log plot of $P(f)$ versus $f$ and find the slope $\beta$ of the linear portion.

Step 4: Estimate the fractal dimension $D$ using the relationship:

$$D = \frac{E - \beta}{2} \tag{3}$$

where $E$ is the Euclidean dimension of the space (e.g., $E = 2$ for a 2D dataset). This method works well for isotropic fractals, where the pattern does not depend on direction.

#### 3.1.2. Box-Counting Method

The box-counting method is one of the most widely used techniques for fractal dimension estimation, particularly for binary and grayscale images. It involves overlaying a grid of square boxes over the data and counting the number of boxes that intersect with the fractal structure [19].

Step 1: Divide the dataset into a grid with box size $\epsilon$.

Step 2: Count the number of boxes $N(\epsilon)$ that contain any part of the fractal structure.

Step 3: Repeat this for various box sizes $\epsilon$.

Step 4: Plot $\log N(\epsilon)$ versus $\log \epsilon$ and calculate the slope of the linear region.

Step 5: The fractal dimension $D$ is given by:

$$D = -\lim_{\epsilon \to 0} \frac{\log N(\epsilon)}{\log \epsilon} \tag{4}$$

In practice, this is approximated numerically. This method is straightforward but can be computationally expensive for large datasets or high-resolution images.

#### 3.1.3. Fast Fourier Transform with Pre-Processing

The pre-processed FFT variant combines pre-processing steps with the FFT method to improve accuracy by reducing noise and highlighting the relevant fractal features. The pre-processing improves the signal-to-noise ratio and ensures a more accurate estimation of the fractal dimension [18]. Common pre-processing steps include the following:

(i) **Thresholding:** Converts greyscale images to binary images.
(ii) **Noise Reduction:** Removes noise using a Gaussian filter.
(iii) **Edge Detection:** Emphasizes significant structure using methods such as Sobel or Canny edge detectors.

Step 1: Pre-process the image or data to emphasize the fractal structure.

Step 2: Compute the power spectrum $P(f)$ using FFT, as described earlier:

$$P(f) = |\mathcal{F}(f)|^2 \tag{5}$$

Step 3: Create a log–log plot of $P(f)$ versus $f$, focusing on the linear region.

Step 4: Calculate the slope $\beta$ of the log-log plot.

Step 5: Estimate the fractal dimension using:

$$D = \frac{E - \beta}{2} \tag{6}$$

where $E$ is the Euclidean dimension of the space. Pre-processing ensures that irrelevant details, such as noise and artifacts, do not distort the estimated fractal dimension.

### *3.2. Chaotic and Fractal Functional Connectivity Analysis*

CFFC matrices provide a novel framework for detecting orthodontic growth and development stages. This innovative approach uses the mathematical principles of chaos theory and fractal geometry to analyze complex patterns within datasets. The method

constructs connectivity matrices using time series generated by chaotic maps and then evaluates their fractal properties to capture the underlying complexity and self-similar structure of the data. The use of 10 chaotic maps, listed in Table 1, forms the basis of this analysis. These maps generate time series that simulate intricate patterns, which are subsequently used to compute connectivity matrices.

**Table 1.** Definition of chaotic maps used to generate CFFC matrix.

| No | Name | Description | Range |
|---|---|---|---|
| 1 | Chebyshev | $d_{t+1} = cos\left(0.5cos^{-1}d_t\right)$ | $(-1,1)$ |
| 2 | Circle | $d_{t+1} = mod\left(d_t + 0.2 - \left(\frac{0.5}{2\pi}\right)sin(2\pi d_t), 1\right)$ | $(0,1)$ |
| 3 | Gauss/mouse | $d_{t+1} = \begin{cases} 1 & for \quad d_t = 0 \\ \frac{1}{mod(d_t,1)} & , \quad otherwise \end{cases}$ | $(0,1)$ |
| 4 | Iterative | $d_{t+1} = sin\left(\frac{0.7\pi}{d_t}\right)$ | $(-1,1)$ |
| 5 | Logistic | $d_{t+1} = \mu d_t(1-d_t) \quad and \quad \mu = 4$ | $(0,1)$ |
| 6 | Piecewise | $d_{t+1} = \begin{cases} \frac{d_t}{0.4} & for \quad 0 \leq d_t < 0.4 \\ \frac{d_t - 1}{0.1} & for \quad 0.4 \leq d_t < 0.5 \\ \frac{0.6 - d_t}{0.1} & for \quad 0.5 \leq d_t < 0.6 \\ \frac{1 - d_t}{0.4} & for \quad 0.6 \leq d_t < 1 \end{cases}$ | $(0,1)$ |
| 7 | Sine | $d_{t+1} = \sin(\pi d_t)$ | $(0,1)$ |
| 8 | Singer | $d_{t+1} = 1.07\left(7.86d_t - 23.31{d_t}^2 + 28.75{d_t}^3 - 13.302875{d_t}^4\right)$ | $(0,1)$ |
| 9 | Sinusoidal | $d_{t+1} = 2.3{d_t}^2 \sin(\pi d_t)$ | $(0,1)$ |
| 10 | Tent | $d_{t+1} = \begin{cases} \frac{d_t}{0.7} & for \quad d_t < 0.7 \\ \frac{10}{3}(1-d_t) & for \quad d_t \geq 0.7 \end{cases}$ | $(0,1)$ |

#### 3.2.1. Chaotic Maps for 1D Signal Generation

Chaotic maps are deterministic systems that exhibit a sensitive dependence on initial conditions, making them ideal for modeling nonlinear and complex behaviors. This method uses 10 chaotic maps, which are described in detail in Table 1. Each map generates a time series that forms the basis for the calculation of connectivity matrices.

#### 3.2.2. Constructing Chaotic and Fractal Functional Connectivity Matrices

CFFC matrices represent the relationships between different signals or regions derived from chaotic maps and fractal dimension-generated 1D signals. The connectivity values between two time series are calculated using measures such as correlation or mutual information.

The Pearson correlation coefficient (PCC) is a measure of the linear relationship between two variables and is calculated by dividing the covariance of the variables by the product of their standard deviations [30]:

$$cov(X,Y) = E[(X - \theta_X)(Y - \theta_Y)] \tag{7}$$

where $E[\cdot]$ is the expectation operator representing the mean of the product, while $\theta_X$ and $\theta_Y$ denote the mean values of $X$ and $Y$, respectively. The PCC is then defined as follows:

$$P_{X,Y} = \frac{cov(X,Y)}{\vartheta_X \times \vartheta_Y} \tag{8}$$

where $P_{X,Y}$ is the PCC between $X$ and $Y$, $cov(X, Y)$ represents the covariance between the two signals as defined in Equation (7), and $\vartheta_X$ and $\vartheta_Y$ denote the standard deviations of $X$ and $Y$, respectively. To generate the CFFC matrix, the fractal dimension of each image is divided by the one-dimensional signal obtained from the original image. To further enrich the analysis, the fractal dimension-normalized signals are aggregated with the chaotic time series generated by the 10 chaotic maps from Table 1. This process produces the CFFC matrix, which combines fractal and chaotic properties and provides a more detailed representation of the underlying patterns.

### *3.3. Wrapper-Based Feature Selection with Puma Optimization*

Feature selection is a crucial step in machine learning, as it improves model performance by eliminating irrelevant or redundant features. In this study, a wrapper-based feature selection approach is employed using the kNN algorithm as the evaluator and the PO algorithm as the search strategy. This combination ensures the selection of an optimal subset of features that improves classification accuracy while minimizing computational complexity.

#### 3.3.1. Puma Optimization Algorithm

The PO algorithm is a metaheuristic algorithm inspired by the hunting strategies of pumas, in particular their ability to explore new territories and exploit known regions efficiently. It is designed to solve optimization problems characterized by large search spaces, nonlinear dynamics, and the presence of local optima. The PO algorithm models the natural hunting behaviors of pumas by incorporating two main phases: exploration, where new territories are sought, and exploitation, where prey is ambushed in known regions. These phases are dynamically balanced by an innovative phase-change mechanism. The mathematical framework of the PO algorithm is presented below, together with an analysis of its main advantages and computational complexity [31].

(i) initialization

The search space is represented by a population of solutions ($X_i$) within predefined bounds:

$$X_i = rand \times (Ub - Lb) + Lb \tag{9}$$

where *rand* is a random number in the range $[0, 1]$, and $Ub$ and $Lb$ represent the upper and lower bounds of the search space, respectively.

(ii) phase-change mechanism

Pumas intelligently switch between exploration and exploitation based on a scoring system. Scores are calculated for each phase using weighted functions:

$$Score_{Explore} = PF_1 \cdot f_1 + PF_2 \cdot f_2 + PF_3 \cdot f_3 \tag{10}$$

$$Score_{Exploit} = PF_1 \cdot f_1 + PF_2 \cdot f_2 + PF_3 \cdot f_3 \tag{11}$$

where $PF_1$, $PF_2$, and $PF_3$ are weighting factors for each function, set between 0 and 1, and $f_1$, $f_2$, and $f_3$ represent functions measuring phase performance based on cost reductions and diversity, with the phase having the higher score being prioritized in subsequent iterations.

(iii) exploration phase

In exploration, pumas randomly search the space using two strategies:

- random jumps:

$$Z_{i,G} = rand \times (Ub - Lb) + Lb \tag{12}$$

- guided search:

$$Z_{i,G} = X_a + G \cdot (X_b - X_c) \tag{13}$$

where $X_a$, $X_b$, and $X_c$ random solutions from the population, and $G = 2 \cdot rand - 1$. Improved solutions are updated based on the cost difference:

$$X_{new} = \begin{cases} Z_{i,G}, & if \quad Cost(Z_{i,G}) < Cost(X_i) \\ X_i, & otherwise \end{cases} \tag{14}$$

(iv) exploitation phase

In exploitation, pumas mimic hunting behaviors such as ambushing and sprinting:

- short jumps (ambush):

$$X_{new} = mean\ (Solutions) - \alpha \cdot (X_i - P_{male}) \tag{15}$$

where $P_{male}$ is the best solution found.

- long jumps (sprint):

$$X_{new} = P_{male} + \gamma \cdot exp(rand) \cdot (X_r - X_i) \tag{16}$$

where $\alpha$ and $\gamma$ are scaling parameters, $X_r$ is a random solution, and solutions are updated if the cost of the new solution is better.

$$X_i = X_{new},\ if\ Cost(Z_{i,G}) < Cost(X_i) \tag{17}$$

The algorithm iterates through the exploration and exploitation phases until a stopping criterion is met. The stopping criterion can be as follows:

Maximum number of iterations (MaxIter)

- Convergence, where the cost difference between iterations becomes negligible.

Although the PO algorithm can be complex to implement, it generally has a low computational complexity, which varies depending on the phase being executed, as each stage has its specific computational requirements. The overall computational complexity of the PO algorithm can be broken down into three main components: initialization, fitness evaluation, and generation of new solutions.

For a population size $N$, the computational complexity during the initialization phase is $O(N)$. In the exploitation phase, which involves generating new solutions, identifying the best location, and updating the position vectors of all pumas, the complexity is $O(N \cdot (T + T \cdot D))$, where $T$ is the maximum number of iterations and $D$ is the dimensionality of the problem.

In the exploration phase, the complexity associated with generating and applying the alternation mechanism is $O((2T + 1) \cdot N \cdot D)$. However, as the exploration phase requires sorting, the worst-case complexity for this operation is $O(N^2)$. As a result, the overall complexity of the exploration phase becomes $O((2T + 1) \cdot N^2 \cdot D)$.

#### 3.3.2. Feature Selection

The CFFC matrices, constructed from the fractal dimensions and correlations of vertebrae images, represent a highly nonlinear dataset. To effectively explore this complex feature space and identify the most relevant features, the exploration phase of the PO algorithm is used. In this study, PO is used to optimize feature selection within the CFFC matrices derived from cervical vertebrae images. By efficiently handling the nonlinear dynamics and computational complexity of the data, the algorithm achieves high classifica-

tion accuracy while minimizing the feature set. This highlights the practical effectiveness of PO in addressing challenges in medical imaging and machine learning applications.

### *3.4. Classification with k-Nearest Neighbors*

The kNN algorithm is a widely used supervised machine learning technique, primarily applied to classification and regression tasks. In classification, the algorithm groups data points based on their similarity, which is determined by a distance function. Commonly used distance measures include Euclidean distance, Hamming distance, and Minkowski distance. The two key factors that influence the decision-making process in kNN are the number of neighbors considered ($k$) and the majority vote among these nearest neighbors. The kNN algorithm works in two main steps: First, it calculates the distances between the target data point and all other points in the dataset to identify the k-nearest neighbors. Second, it classifies the target point based on the majority label among these neighbors. Unlike many other algorithms, kNN does not require a separate training phase to build a model. This feature significantly reduces both time and computational cost, making it a lightweight yet effective method [32,33].

In this study, the kNN algorithm is used to classify orthodontic growth and development stages, providing an efficient approach that combines high accuracy with low computational overhead. The classification process starts with the selection of features optimized by the PO algorithm. The features identified by the PO algorithm are fed into the kNN classifier. The PO exploitation phase plays a crucial role in ensuring that the selected features improve the performance of the classifier by iteratively refining the feature set. This integration of PO and kNN not only streamlines the feature selection process but also ensures that the classifier operates on the most relevant and influential features, leading to accurate and efficient classification results.

### *3.5. Performance Metrics for Classification*

The dataset used in this study consists of cervical vertebrae images and is randomly divided into two independent subsets: 90% of the data are used for training, while the remaining 10% are reserved for testing. To assess the effectiveness of the models developed for the classification of orthodontic growth and developmental stages, the study uses a robust 10-fold cross-validation approach. This method involves dividing the training dataset into ten equal parts, using nine parts for training and one part for validation in each iteration. The performance of the model is evaluated by computing the average accuracy from all ten folds, ensuring a comprehensive and unbiased assessment.

The study evaluates the classification performance on the test set using several metrics derived from the confusion matrix, as defined in Equations (18)–(21). The confusion matrix uses four key terms: true positives (TPs), which represent correctly identified positive samples; false positives (FPs), indicating samples incorrectly predicted as positive; true negatives (TNs), representing correctly identified negative samples; and false negatives (FNs), which are positive samples that were incorrectly classified as negative. These metrics provide a multi-faceted evaluation of the classification model's capabilities.

$$\text{Acc} = \frac{TP + TN}{TP + TN + FP + FN}, \tag{18}$$

$$\text{Prec} = \frac{TP}{TP + FP}, \tag{19}$$

$$\text{Rec} = \frac{TP}{TP + FN}, \tag{20}$$

$$\text{F1-score} = \frac{2 \times Recall \times Precision}{Recall + Precision}. \tag{21}$$

Acc is one of the primary metrics and measures the proportion of correct predictions out of the total predictions made by the classifier. It is calculated as the ratio of the sum of true positives and true negatives to the total number of samples. Acc provides an overall measure of the classifier's ability to make correct predictions across all classes. *Prec* measures the accuracy of positive predictions. It is calculated by dividing the number of true positives by the total number of samples predicted as positive (true positives + false positives). Prec reflects the model's ability to avoid false-positive errors, making it particularly important in applications where incorrect positive predictions have significant consequences. Rec, also known as sensitivity, quantifies the ability of the model to correctly identify true positive samples. It is determined by dividing the true positives by the total number of actual positives (true positives + false negatives). A high recall score indicates that the classifier is effective in identifying positive instances. The F1-score is a harmonic mean of precision and recall, providing a balanced assessment of the classifier's performance. This metric is particularly valuable in scenarios with unbalanced datasets, where the number of positive and negative samples differs significantly. By combining Prec and Rec, the F1-score provides insight into the trade-off between these two metrics, ensuring a comprehensive assessment of the model's effectiveness [34].

This study uses a combination of cross-validation, Acc, Prec, Rec, and F1-score to provide a thorough and detailed evaluation of the classifiers, providing valuable insights into their effectiveness and reliability in classifying orthodontic growth and development stages.

### *3.6. Framework of the Proposed Orthodontic Growth and Development Stage Classification Model*

In this study, we propose a robust hybrid model designed to classify orthodontic growth and development stages with high accuracy, minimal computational cost, and reduced model complexity, while taking into account the nonlinear dynamics inherent in medical imaging. The framework of the proposed model is illustrated in Figure 1, and the processing steps are briefly outlined below:

Step 1: In the data preparation phase, 30 × 30 pixel images centered on the C2, C3, and C4 vertebrae bodies are extracted from two-dimensional lateral cephalometric radiographs taken during the pre-peak, peak, and post-peak skeletal growth stages. These images are used for orthodontic purposes to identify skeletal growth and development stages. The dataset is then split into 90% training data and 10% test data to ensure independence between the subsets.

Step 2: Three different fractal analysis methods, FFT, box counting, and the pre-processed FFT variant, were used to assess the surface complexity of the C2, C3, and C4 vertebrae bodies. These methods were used to calculate the fractal dimensional values of each vertebra, allowing comparison of surface complexity levels and providing baseline data for subsequent signal processing.

Step 3: For each growth stage, the 30 × 30 pixel two-dimensional vertebrae images were reduced to one-dimensional signals in order to analyze the connections between the C2, C3, and C4 vertebral bodies. This dimensional reduction provided the basis for evaluating vertebral pair correlations and constructing connectivity matrices to be used in the classification steps.

Step 4: In this step, basic functional connectivity (FC) was first established by calculating the PCC between the original signals. The one-dimensional signals were then normalized using fractal dimension values derived from fractal analyses, and a new PCC calculation was performed to generate fractal FC matrices. Finally, the normalized signals were combined with 10 different chaotic maps, shown in Table 1, and PCC calculations were repeated to construct chaotic FC matrices.

Step 5: Feature selection was performed to minimize computational complexity and maximize model performance. A wrapper-based approach combining the Puma optimization algorithm and kNN classifiers was used to select optimal features from the lower triangles of the FC matrices, resulting in 36 features. The fitness function was designed to meet these criteria, and the optimization process aimed to achieve maximum classification accuracy with the minimum number of features.

Step 6: The selected optimal feature vectors were fed into the kNN algorithm to classify the pre-peak, peak, and post-peak growth and development stages. The model was validated using 10-fold cross-validation, and its classification performance was evaluated based on *Acc*, *Prec*, *Rec*, and *F1-score* metrics. Additionally, the effectiveness of the model was compared with an SVM classifier to demonstrate its reliability and efficiency.

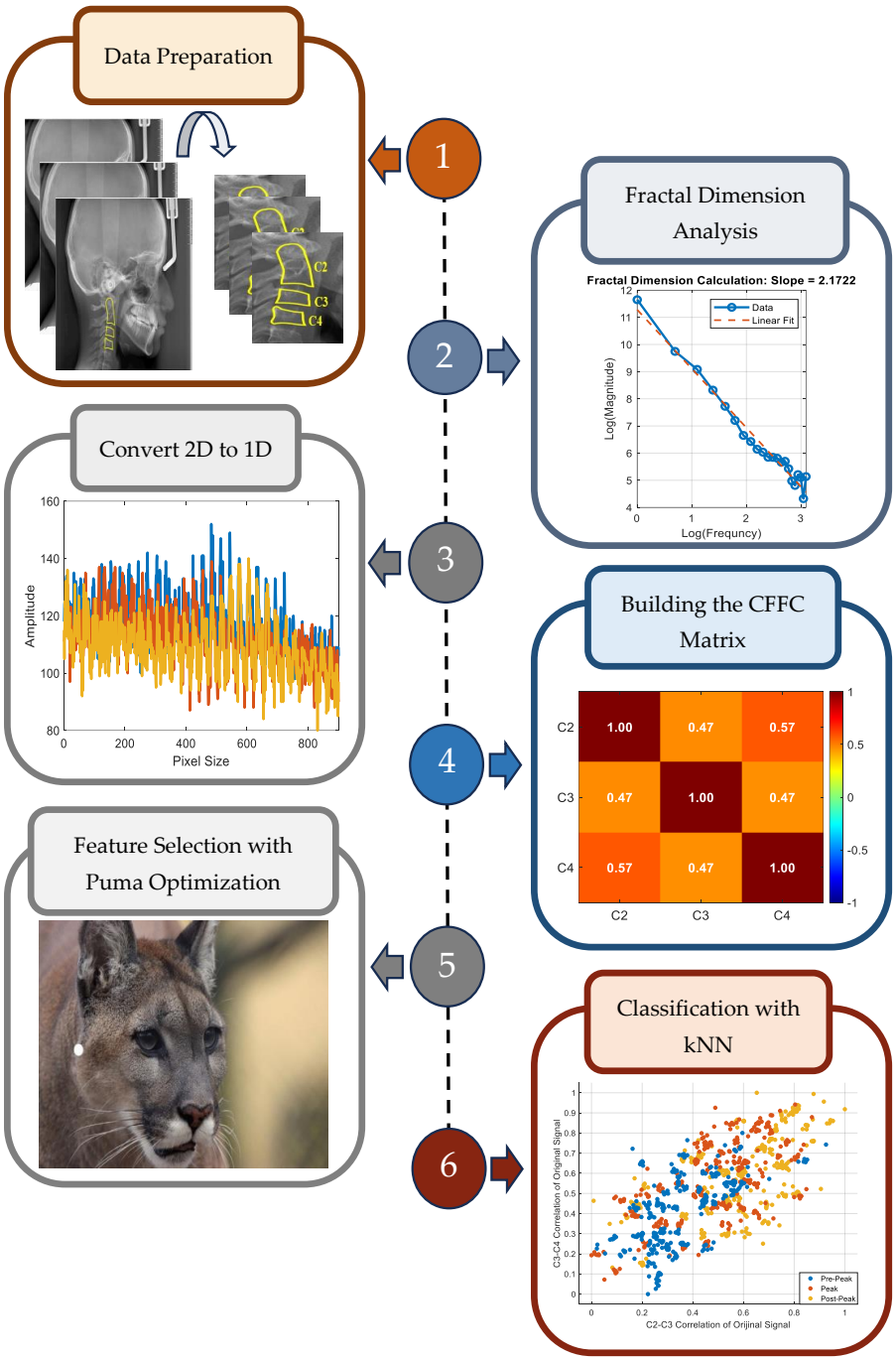



**Figure 1.** Framework of the proposed orthodontic growth stage classification model.

## 4. Results and Discussion

This section presents the evaluation of the performance of the proposed model using a dataset consisting of two-dimensional lateral cephalometric radiographs. The dataset is categorized into three classes, pre-peak, peak, and post-peak, and includes images of the C2, C3, and C4 vertebrae. The chaotic and fractal structures in the C2, C3, and C4 vertebrae were analyzed using three different fractal dimensional analysis methods: FFT, box counting, and the pre-processed FFT variant.

The proposed model includes several steps, including dimensionality reduction of C2, C3, and C4 cervical vertebrae images to one-dimensional signals, feature extraction using fractal dimensions and chaotic maps, feature selection using a wrapper approach combining the PO algorithm and kNN classifier, and classification using the kNN model. The study specifically examines the effect of feature selection, based on fractal dimensions and chaotic maps, on the performance of the model using the PO algorithm for each fractal dimension analysis method. Additionally, the performance of the kNN-based classification model is compared with that of a model constructed using the SVM classifier, providing a comprehensive analysis of the proposed approach.

### *4.1. Dataset*

The dataset used in this study was prepared experimentally at Zonguldak Bülent Ecevit University, Faculty of Dentistry, Department of Orthodontics. Specifically designed for the classification of pre-peak, peak, and post-peak growth and development stages, the dataset was derived from lateral cephalometric radiographs. To focus on the regions relevant to the classification task, the areas containing the C2, C3, and C4 vertebrae were isolated and cropped, as illustrated in Figure 2. This targeted approach ensured that the dataset emphasized the anatomical structures essential for growth and development stage analysis. The dataset was divided into three distinct classes: pre-peak, peak, and post-peak growth stages. As shown in Figure 3, each class included images of the C2, C3, and C4 vertebrae. For each vertebrae type, 315 images were included per stage, resulting in a total of 945 images for each stage and 2835 images for the entire dataset. The balanced distribution across classes ensured that all vertebral types were equally represented, minimizing bias and improving stage classification accuracy.

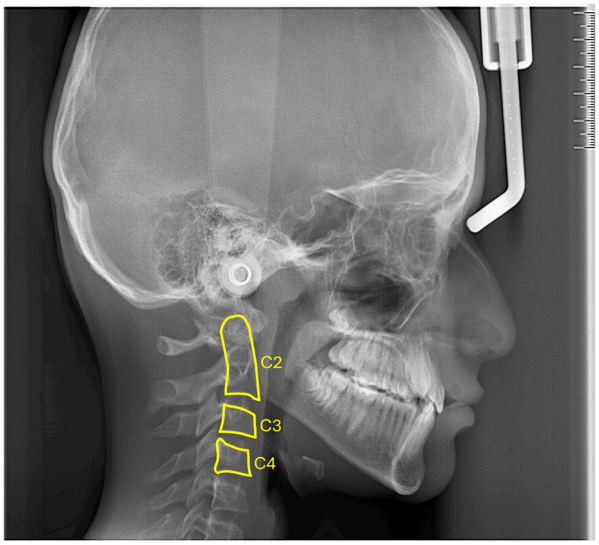



**Figure 2.** Representation of the cropped C2, C3, and C4 vertebrae regions on a lateral cephalometric radiograph.

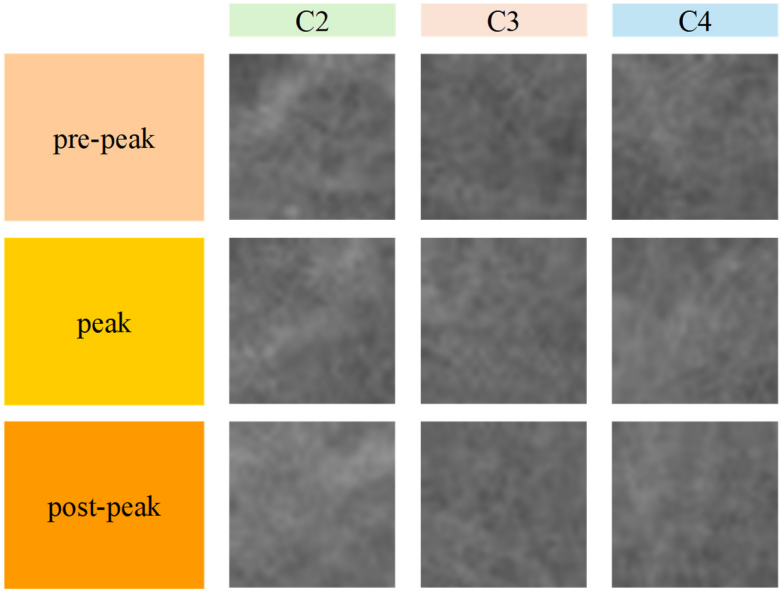



**Figure 3.** A sample of a dataset of C2, C3, and C4 vertebrae images for pre-peak, peak, and post-peak growth stages.

In addition to analyzing each vertebrae type individually, the study also evaluated the correlations between the C2, C3, and C4 vertebrae. This approach allowed a comprehensive analysis of the functional connections between the vertebrae, providing valuable insights into the differences between growth stages. By considering all vertebrae types together, the dataset enabled a holistic classification strategy that exploited the relationships between 945 vertebrae images at each stage. For model training and testing, the dataset was randomly divided into two independent subsets. About 90% of the images were used for training, while the remaining 10% were reserved for testing. To reduce computational complexity and streamline the fractal dimension analysis, all vertebrae images were cropped to a uniform size of 30 × 30 pixels, with the cropping centered on the vertebral regions of interest. This pre-processing step preserved critical features while increasing computational efficiency.

The inclusion criteria for lateral cephalometric radiographs are as follows: (i) lateral cephalometric radiographs taken in a natural head position and belonging to the pre-peak, peak, and post-peak growth and development stages; (ii) high-resolution lateral cephalometric radiographs that clearly show the second to fourth cervical vertebrae (C2, C3, and C4); and (iii) the absence of any congenital or developmental deformity or systemic bone disease of the vertebrae. Radiographs with poor image quality that did not meet at least one of these criteria were excluded from the study.

### *4.2. Fractal Dimension Analysis with FFT, Box Counting, and Pre-Processed FFT*

The density and structural complexity of cervical vertebrae undergo significant changes during different stages of growth and development. These changes can be assessed quantitatively using fractal dimensional analysis, which provides numerical insights into structural variation. The fractal theory is widely used to evaluate surface density, structural complexity, and irregularity by analyzing pixels or geometric shapes that exhibit complex, self-similar, and irregular patterns at different scales. In this study, the fractal dimensions of C2, C3, and C4 cervical vertebrae images, corresponding to the pre-peak, peak, and post-peak growth stages, were measured using three methods: FFT, box counting, and pre-processed FFT. A sample of the fractal dimension measured by each method is shown in Figures 4–6, respectively.

The inclusion of three fractal dimension calculation methods—FFT, box counting, and pre-processed FFT—serves both as a means to improve feature extraction and as a comparative analysis of their effectiveness in capturing the fractal characteristics of cervical vertebrae. By evaluating their individual contribution to feature selection and classification accuracy, we aim to determine the most effective approach to modeling non-linear growth dynamics. This comparison will ensure a more robust and comprehensive framework for vertebral analysis.

The structural differences and fractal characteristics of C2, C3, and C4 vertebrae at each growth stage were analyzed using these methods. The average fractal dimensions measured for each growth stage and vertebrae type using the FFT, box counting, and pre-processed FFT methods are presented in Table 2. This detailed analysis highlights the structural variations and levels of complexity of the cervical vertebrae associated with pre-peak, peak, and post-peak growth stages.

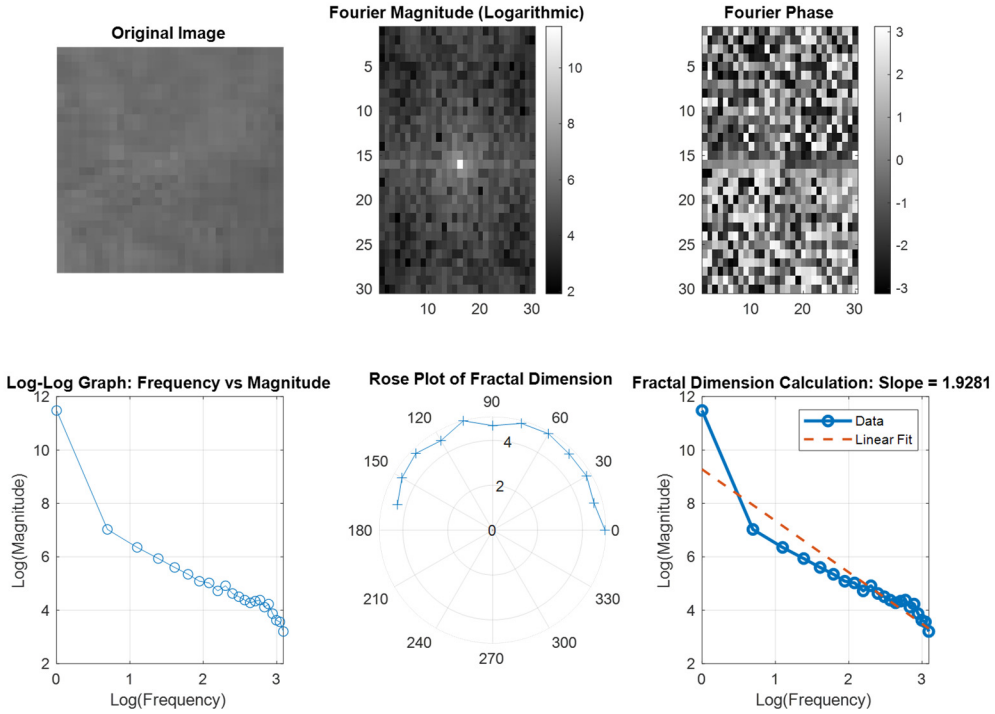



**Figure 4.** Sample of fractal dimension measurement of cervical vertebrae using the FFT method.

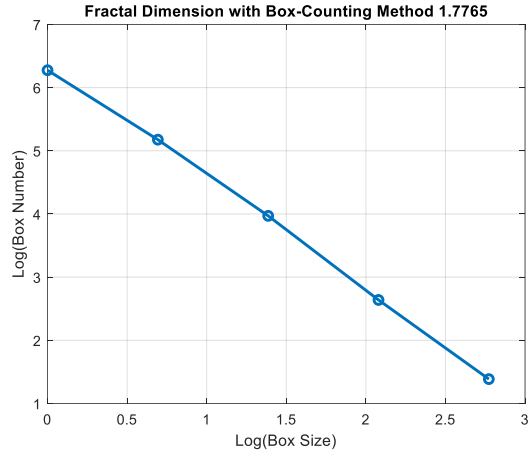



**Figure 5.** Sample of fractal dimension measurement of cervical vertebrae using the box-counting method.

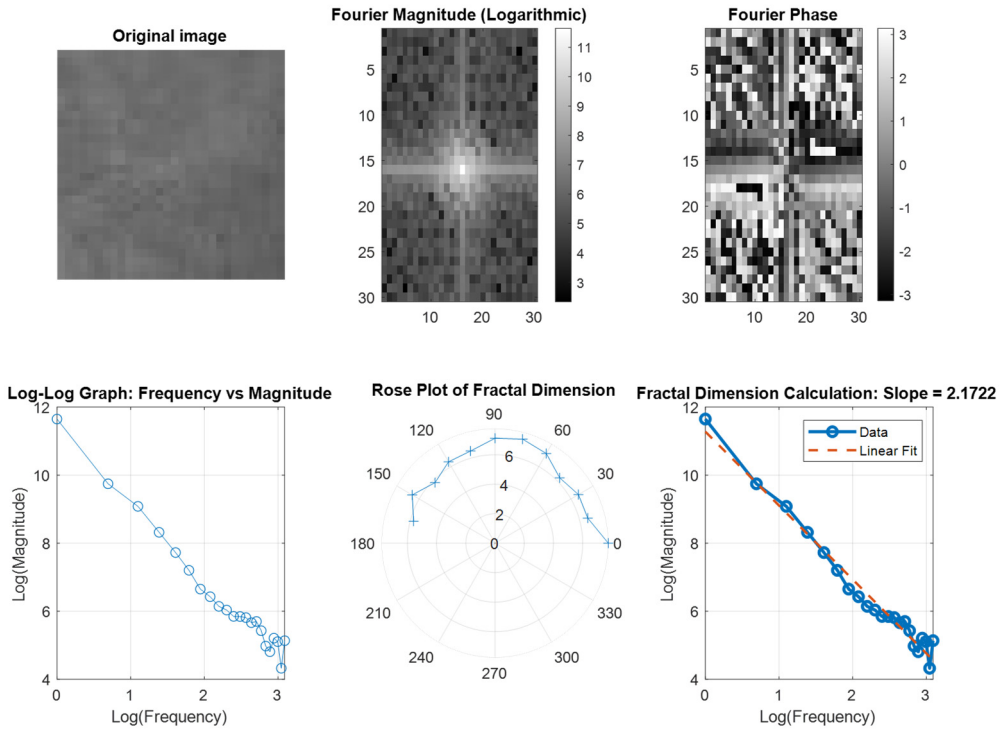



**Figure 6.** Sample of fractal dimension measurement of cervical vertebrae using the pre-processed FFT method.

**Table 2.** Mean fractal dimensions of C2, C3, and C4 cervical vertebrae for pre-peak, peak, and post-peak growth and development stages using FFT, box counting, and pre-processed FFT methods.

| Methods | Pre-Peak | | | Peak | | | Post-Peak | | |
|---|---|---|---|---|---|---|---|---|---|
| | C2 | C3 | C4 | C2 | C3 | C4 | C2 | C3 | C4 |
| FFT | 1.97 | 1.93 | 1.95 | 1.95 | 1.91 | 1.92 | 1.99 | 1.92 | 1.94 |
| Box counting | 1.64 | 1.61 | 1.64 | 1.61 | 1.64 | 1.63 | 1.65 | 1.66 | 1.67 |
| Pre-processed FFT | 2.23 | 2.12 | 2.18 | 2.21 | 2.16 | 2.20 | 2.27 | 2.20 | 2.23 |

The analysis of the average fractal dimensions presented in Table 2 shows significant differences between the methods used and the growth stages. The fractal dimensions measured by the box-counting method ranged between 1.61 and 1.67, consistently yielding lower values than the other methods. Minimal differences were observed between vertebrae in the pre-peak and peak classes. The fractal dimensions for C2, C3, and C4 in the pre-peak class were 1.61, 1.62, and 1.63, respectively, while in the peak class, these values were 1.63, 1.62, and 1.64. These small differences indicate a high degree of similarity in surface complexity within these two classes. However, a slight increase was observed in the post-peak class, particularly for C3 and C4, where the fractal dimensions were 1.66 and 1.67, respectively. This increase suggests that the vertebral surfaces become more complex and irregular during the post-peak stage, highlighting structural changes that become more pronounced during this stage. These results demonstrate that while the box-counting method provides a general indication of surface complexity and density, it has limited sensitivity for detecting subtle differences.

The fractal dimensions calculated using the FFT method ranged from 1.91 to 1.99, providing higher values compared to the box-counting method. In the pre-peak class, the fractal dimensions of C2, C3, and C4 were 1.97, 1.92, and 1.94, respectively. The highest fractal dimension observed for C2 indicates that its surface complexity was greater than that of the other vertebrae at this stage. In the peak class, the differences were more pronounced;

C2 had the highest fractal dimension with a value of 1.95, while C3 had the lowest with a value of 1.91. This indicates that the surface complexity of C3 is comparatively lower at this stage. In the post-peak class, the fractal dimensions for C2, C3, and C4 were 1.99, 1.94, and 1.96, respectively. C2 had the highest fractal dimension, indicating a significant increase in surface complexity for this vertebra during the post-peak phase. These results highlight the high sensitivity of the FFT method in analyzing structural variations and surface complexity of vertebrae at different growth stages.

The fractal dimensions measured using the pre-processed FFT method ranged from 2.12 to 2.27, giving the highest values of the three methods. In the pre-peak class, the fractal dimensions of C2, C3, and C4 were 2.23, 2.18, and 2.20, respectively. The highest value observed for C2 suggests that its surface details are more pronounced compared to the other vertebrae at this stage. In the peak class, the fractal dimensions for C2, C3, and C4 were 2.21, 2.16, and 2.20, respectively, showing minimal differences between the vertebrae. This indicates that the surfaces are structurally similar and homogeneous in complexity at this stage. A significant increase in fractal dimensions was observed in the post-peak class. The values for C2, C3, and C4 were 2.27, 2.22, and 2.23, respectively, with C2 having the highest fractal dimension. This reflects a marked increase in surface complexity for C2 during the post-peak stage, while the increased complexity of C4 also highlights structural changes in this vertebra. The results obtained using the pre-processed FFT method demonstrate its superior ability to analyze the structural differences and surface details of vertebrae.

In the pre-peak and peak classes, the differences in fractal dimension between vertebrae were relatively small, reflecting a high degree of similarity in surface complexity between these growth stages. However, in the post-peak class, a significant increase in fractal dimension values was observed for C3 and C4 compared to their counterparts in the pre-peak and peak classes. For example, the fractal dimension of C3 increased from 1.62 in the pre-peak class to 1.94 in the post-peak class when analyzed using the FFT method. Similarly, the fractal dimension of C4 increased from 1.63 to 1.96. These results indicate that the surface complexity of the vertebrae increases significantly during the post-peak stage, with structural changes becoming more pronounced. When comparing vertebrae, the C2 vertebra consistently showed greater surface complexity in the pre-peak and peak classes. For example, in the pre-peak stage, the fractal dimension of C2 measured using the pre-processed FFT method was 2.23, which was higher than the dimensions for C3 and C4. In the post-peak stage, the increased complexity of C3 and C4 vertebrae, with fractal dimensions of 2.22 and 2.23, respectively, indicates more substantial structural changes in these vertebrae.

These results suggest that the changes in vertebral surface complexity across different growth stages reflect stage-specific structural variations, providing valuable insights into the growth-related transformations of cervical vertebrae.

### *4.3. Construction of Functional Connectivity Matrices Based on PCC, Fractal Dimensions, and Chaotic Maps*

To analyze the connections between the C2, C3, and C4 vertebral bodies across different growth stages, the two-dimensional vertebrae images ($30 \times 30$ pixels) were reduced to one-dimensional signals. This dimensional reduction allowed the evaluation of pairwise correlations between vertebrae and the construction of connectivity matrices, which were subsequently used in the classification process.

The first step was to establish FC by calculating the PCC between the original one-dimensional signals. The signals were then normalized using fractal dimension values obtained from fractal analysis. A new PCC calculation was then performed on the normalized signals, resulting in the generation of fractal FC matrices. To further refine the connectivity analysis, normalized signals were combined with 10 different chaotic maps,

as outlined in Table 1, which allowed the construction of chaotic FC matrices. By integrating chaotic maps into the signals, a new signal was generated for each map, which was then used to construct chaotic map-based FC matrices. This approach facilitated the investigation of the influence of chaotic structures on intervertebral connectivity. The process was repeated ten times for each class, resulting in a total of 30 chaotic map-based FC matrices, providing a deeper understanding of how chaotic dynamics affect FC in vertebral structures.

For each growth and development stage, $3 \times 3$ CFFC matrices were created by calculating the PCC between the signals of vertebral pairs, as illustrated in Figure 7. These matrices represent the connectivity relationships between the vertebrae, including the C2–C3, C2–C4, and C3–C4 pairs. The CFFC matrices provide a detailed representation of the intervertebral relationships, highlighting the structural and functional connections between vertebrae at different stages of growth.

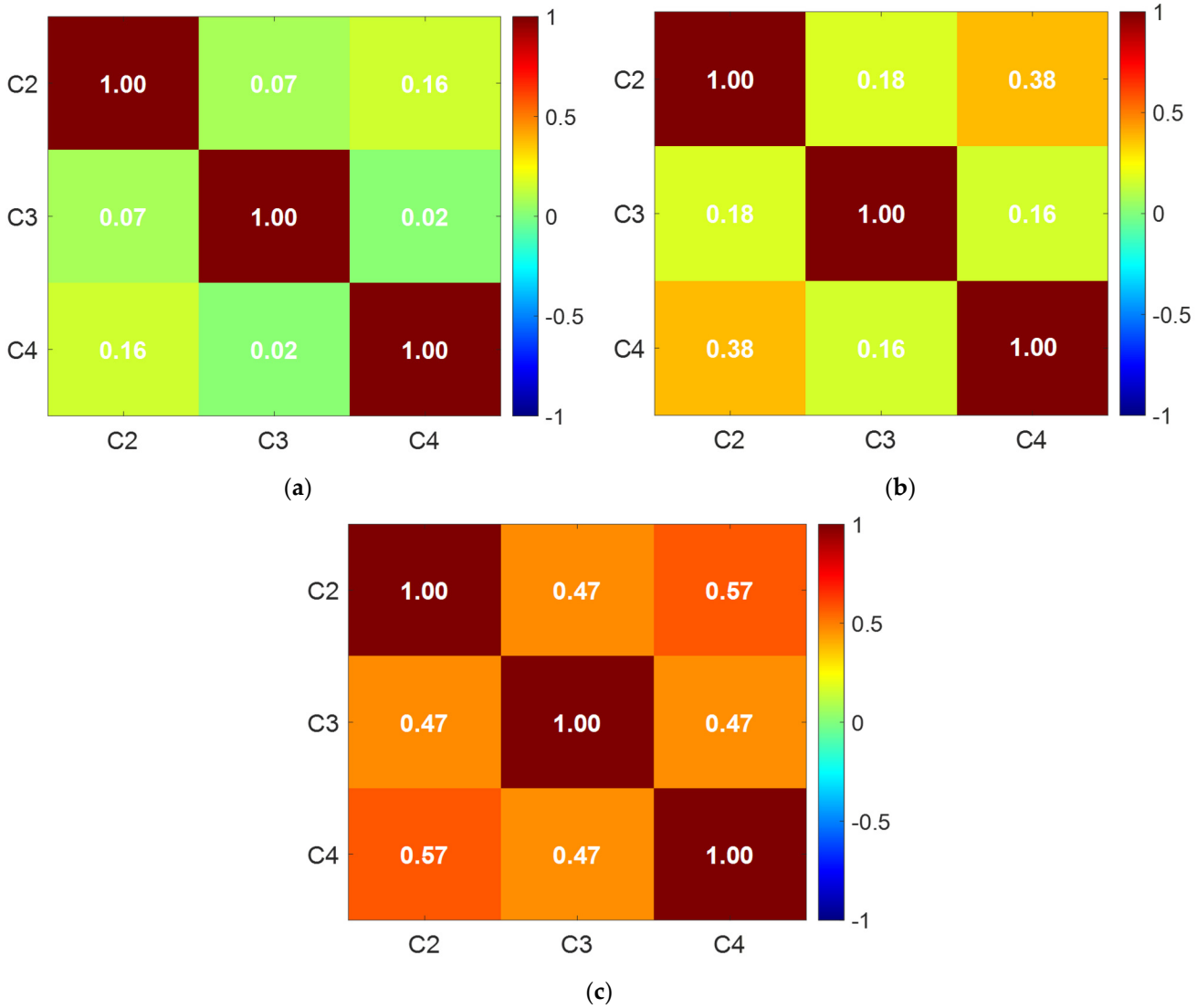



**Figure 7.** A sample of CFFC matrices for growth and development stages: (**a**) pre-peak stage, (**b**) peak stage, and (**c**) post-peak stage.

All FC matrices were symmetric, and the lower triangular elements of each matrix were extracted to construct feature maps. For each growth stage, pre-peak, peak, and post-peak, the connectivity values derived from the base FC matrices, fractal dimension-based FC matrices, and chaotic map-based FC matrices were combined. This resulted

in a comprehensive feature map consisting of 36 features that captured the connectivity patterns across growth stages. The feature map was then fed into the PO algorithm, which used a wrapper-based approach to feature selection. This process ensured the identification of distinctive and relevant features while reducing the computational cost of classification. By integrating FC analysis with fractal dimensions and chaotic maps, this study provided a deeper understanding of the relationship between structural complexity and connectivity in vertebral surfaces. The proposed method provides a robust framework for investigating connectivity in biological systems, highlighting the intricate connections between structural features and functional relationships.

### *4.4. Feature Selection with Wrapper-Based PO-kNN*

Fractal dimension analysis, combined with chaotic map integrated FC analysis, was used to extract 36 features. However, using all feature groups directly increases model complexity and may reduce classification accuracy by including features that contribute minimally to performance. To minimize model complexity while maintaining high classification accuracy, it is crucial to identify the optimal feature subset.

The PO algorithm, inspired by the hunting behaviors and survival strategies of the puma, was employed to select the most relevant feature subset from normalized feature sets. The selection process was performed using a wrapper-based approach, designed to maintain the high performance of the kNN classifier. This selection is guided by a fitness function that evaluates the trade-off between classification quality and subset size:

$$fitness\ function = \rho \times e_r + \sigma \times \left( \frac{selected\ feature\ subset}{total\ number\ of\ features} \right) \tag{22}$$

Here, $e_r$ represents the classification error of the kNN classifier, while $\rho \in [0, 1]$ and $\sigma \in [1 - \rho]$ denote the importance of classification accuracy and subset size, respectively. The fitness function accounts for both the performance of the model and the features it uses, aiming to reduce model complexity and computational costs.

The parameter values used in the PO-kNN feature selection process are presented in Table 3. These parameters were used in the feature selection process for models created with fractal dimensional analyses (FFT, box counting, and pre-processed FFT) using kNN and SVM classifiers. This process ensured that the selected features were both effective and computationally efficient for the classification tasks.

**Table 3.** Parameter values of the PO-kNN used for the selection of the features.

| Parameters | Value |
|---|---|
| Total number of solutions | 50 |
| Total number of features | 36 |
| Total number of iterations | 100 |
| Fitness function | Maximization of classifier performance and minimization of the number of selected features |

The wrapper-based PO-kNN approach was applied to models generated using fractal analysis methods, and the frequency of feature selection over 100 iterations is shown in Figure 8. Features were indexed from 1 to 36, where indices 1–3 represent correlations between the original signals, indices 4–6 represent correlations derived using fractal dimensions, and indices 7–36 represent correlations incorporating fractal dimensions along with chaotic maps listed in Table 1.

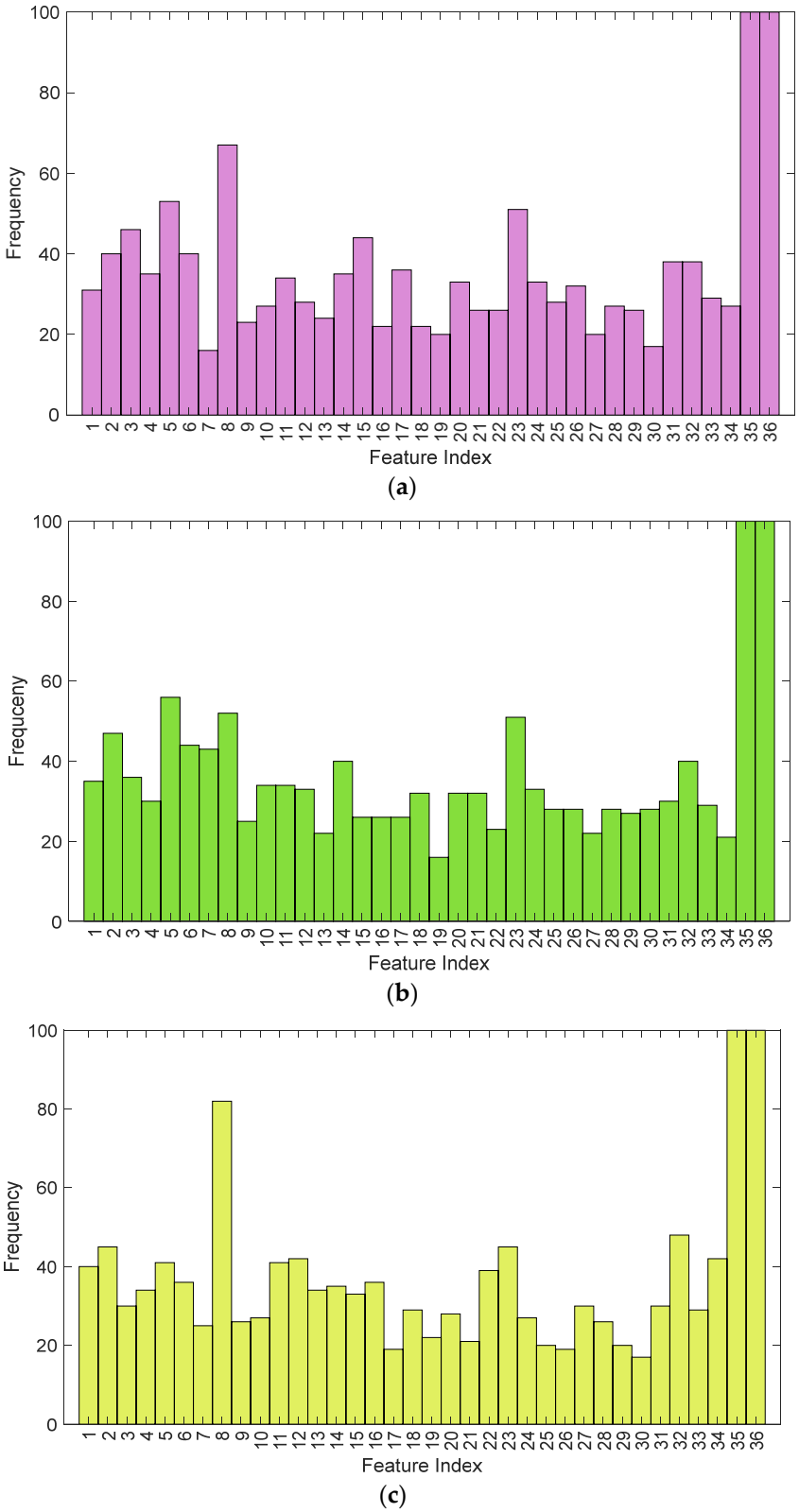



**Figure 8.** Frequencies of feature selection for models based on (**a**) FFT, (**b**) box counting, and (**c**) pre-processed FFT methods over 100 iterations.

In the model developed using the box-counting method, indices 2, 5, 6, 7, 8, 23, 35, and 36 were selected with a frequency of more than 40%. Among them, a balanced distribution was observed, except for indices 35 and 36, which showed higher selection rates. For the FFT-based model, indices 3, 5, 8, 15, 23, 35, and 36 exceeded the 40% selection threshold,

with index 8 reaching a selection frequency of 60%, an increase of 15% compared to the box-counting method. Similarly, in the pre-processed FFT model, indices 2, 5, 8, 11, 12, 23, 32, 35, and 36 were selected with frequencies above 40%, with index 8 showing a 15% higher selection rate compared to the FFT model and a 30% higher rate compared to the box-counting method. This highlights the critical role of feature 8 in the classification process of the pre-processed FFT model. Furthermore, an increased selection frequency for index 32 was observed in this model compared to the other methods.

Across all fractal analysis methods, features representing correlations between the C2–C4 and C3–C4 vertebrae, calculated using fractal dimensions and the Tent chaotic map, were consistently selected in all 100 iterations. This consistency highlights the significance of these features in distinguishing pre-peak, peak, and post-peak growth stages, indicating their critical role in the classification process.

The distribution of the number of features selected over 100 iterations for models generated using fractal analysis methods is illustrated in Figure 9. Out of a total of 36 features, the median number of selected features across all models was found to be 13, indicating that, on average, the models used 13 features in each iteration. For the model constructed using the box-counting method, the feature selection showed a narrower distribution range compared to the models constructed using the FFT and pre-processed FFT methods, which showed a wider range. Specifically, the box-counting-based model selected a minimum of 9 features, whereas the FFT and pre-processed FFT models selected only 7 features. This observation highlights the potential of the FFT and pre-processed FFT methods to maintain high performance with fewer selected features. These methods demonstrate greater flexibility and effectiveness in the classification processes, making them valuable for feature selection and classification tasks.

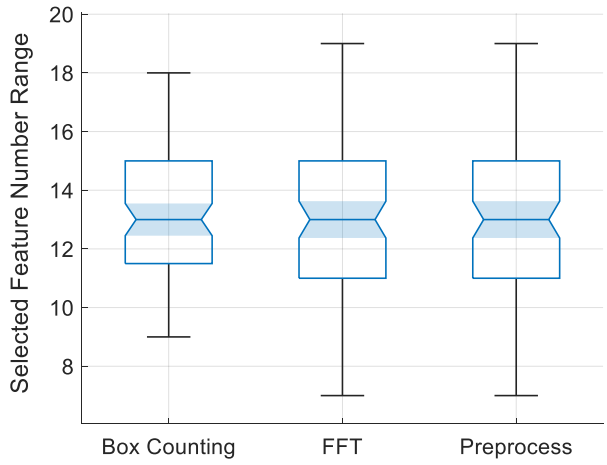



**Figure 9.** Distribution of selected features over 100 iterations using the wrapper-based PO-kNN approach.

### *4.5. Classification*

All pre-peak, peak, and post-peak growth stage classification experiments were performed on a personal computer equipped with an Intel Core i7-12700H CPU, 6 GB NVIDIA GeForce RTX 3060 GPU, and 16 GB RAM. All code was implemented and compiled using MATLAB 2022b. This study investigates the impact of different fractal dimensional analysis methods and chaotic maps on the performance of both optimization and classification algorithms. By systematically analyzing these factors, the study aims to improve the accuracy and efficiency of the proposed classification framework. The parameter values for the proposed classification algorithm, as well as for the other classifiers used in the study, are

detailed in Table 4. These parameters have been optimized to ensure robust and reliable classification performance across all growth stages.

**Table 4.** Parameter values for the proposed and comparative classification algorithms.

| Parameters | kNN | SVM |
|---|---|---|
| Distance | Euclidean | - |
| Number of neighbors | 1 | - |
| Distance weight | Equal | - |
| Kernel function | - | Gaussian |
| Kernel scale | - | 0.71 |
| Box constraint | - | 1 |

The models developed in this study were tested on 94 images for each class. To evaluate the robustness of each model, the testing process was repeated 100 times. In addition, during each iteration, the models were validated using 10-fold cross-validation. The performance of each classification model was calculated by averaging the accuracy values obtained from each fold. The study evaluated the performance of all classification models on the test data using the metrics defined in Equations (18)–(21). The accuracy performance of the kNN and SVM classification models, built using features selected by the PO-kNN wrapper approach based on three different fractal dimension methods, is presented in Table 5. An analysis of all the models in Table 5, based on the accuracy performance metric, showed that the model combining the PO-kNN wrapper approach and the kNN classifier, using features derived from the pre-processed FFT-based fractal dimension method, achieved the highest performance. Therefore, this model is recommended for the classification of pre-peak, peak, and post-peak growth stages. The proposed model achieved an accuracy of 96.30%, demonstrating its effectiveness for growth stage classification. In addition, the low standard deviation observed in the performance of the model further validates its robustness.

**Table 5.** Accuracy performance of classification models based on features selected by the PO-kNN wrapper approach using different fractal dimension methods.

| | FFT | | | Box Counting | | | Pre-processed FFT | | |
|---|---|---|---|---|---|---|---|---|---|
| | **SFN** | **Index** | **Acc** | **SFN** | **Index** | **Acc** | **SFN** | **Index** | **Acc** |
| **kNN** | 7 | 41 | 95.98 ± 0.021 | 9 | 4 | 95.45 ± 0.015 | 7 | 88 | 96.30 ± 0.017 |
| | 8 | 2 | 95.34 ± 0.026 | 9 | 5 | 95.24 ± 0.026 | 8 | 13 | 95.56 ± 0.018 |
| | 9 | 85 | 96.08 ± 0.017 | 9 | 12 | 95.66 ± 0.017 | 8 | 70 | 95.45 ± 0.017 |
| | 9 | 94 | 95.66 ± 0.020 | 9 | 77 | 94.71 ± 0.021 | 9 | 25 | 95.45 ± 0.026 |
| **SVM** | 7 | 41 | 92.91 ± 0.011 | 9 | 4 | 93.23 ± 0.012 | 7 | 88 | 93.02 ± 0.015 |
| | 8 | 2 | 93.76 ± 0.012 | 9 | 5 | 94.07 ± 0.012 | 8 | 13 | 93.23 ± 0.018 |
| | 9 | 85 | 94.29 ± 0.013 | 10 | 60 | 93.33 ± 0.016 | 8 | 70 | 93.33 ± 0.018 |
| | 9 | 94 | 94.18 ± 0.015 | 10 | 96 | 94.39 ± 0.011 | 9 | 47 | 93.86 ± 0.014 |
| | 10 | 23 | 93.44 ± 0.010 | 11 | 9 | 93.33 ± 0.016 | 9 | 25 | 93.86 ± 0.011 |
| | 10 | 38 | 94.18 ± 0.010 | 11 | 84 | 94.60 ± 0.014 | 10 | 44 | 93.44 ± 0.012 |
| | 11 | 73 | 93.33 ± 0.014 | 12 | 17 | 93.33 ± 0.012 | 10 | 31 | 94.18 ± 0.013 |
| | 11 | 11 | 94.39 ± 0.017 | 12 | 6 | 94.07 ± 0.016 | 11 | 28 | 93.33 ± 0.010 |
| | 12 | 8 | 94.07 ± 0.015 | 13 | 58 | 93.33 ± 0.019 | 11 | 16 | 94.39 ± 0.016 |
| | 12 | 99 | 93.44 ± 0.019 | 13 | 76 | 94.29 ± 0.017 | 12 | 39 | 93.12 ± 0.016 |
| | 13 | 100 | 93.23 ± 0.013 | 14 | 97 | 93.33 ± 0.018 | 12 | 30 | 94.07 ± 0.014 |
| | 13 | 13 | 94.50 ± 0.016 | 14 | 34 | 94.07 ± 0.014 | 13 | 48 | 94.29 ± 0.013 |

For the proposed pre-peak, peak, and post-peak classification model based on the pre-processed FFT method and chaotic maps, seven features were selected using the PO-kNN wrapper approach. The selected features included the primary correlation between C2–C3 vertebrae, the fractal-based correlation between C3–C4 vertebrae, and the chaotic map-based correlations between vertebrae in different configurations. Specifically, the selected features were the Chebyshev chaotic map-based correlation for C2–C4 vertebrae, Circle chaotic map-based correlation for C2–C4 vertebrae, Sinusoidal chaotic map-based correlation for C2–C4 vertebrae, Tent chaotic map-based correlation for C2–C4 vertebrae, and Tent chaotic map-based correlation for C3–C4 vertebrae. These results highlight the critical role of the pre-processed FFT method and chaotic maps in improving classification performance. The selected features effectively capture the complex relationships and structural differences between vertebral surfaces that are essential for accurate classification. Notably, the proposed model demonstrated superior performance compared to other models while using a minimal number of features. This result highlights the efficiency of the proposed model in achieving high classification accuracy with lower computational cost. The ability of the model to achieve optimal performance with fewer selected features demonstrates the effectiveness of the optimization process in dealing with nonlinear dynamics.

The classification performance of the proposed model and a comparative SVM-based model for the pre-peak, peak, and post-peak growth stages is illustrated by the confusion matrices in Figure 10. The proposed model achieved classification accuracies of 98.4% for the pre-peak stage, 95.3% for the peak stage, and 95.2% for the post-peak stage. In comparison, the SVM-based model achieved accuracies of 98.1% for the pre-peak stage, 89.9% for the peak stage, and 91.4% for the post-peak stage. While both models performed well at the pre-peak stage, achieving over 98% accuracy, the proposed model outperformed the SVM-based model at the peak and post-peak stages by 5.4% and 3.8%, respectively. These results indicate that the SVM-based model had a higher rate of misclassification rate at the peak and post-peak stages, often assigning samples to two or more incorrect classes. This limitation negatively affects the reliability of the SVM-based model. In contrast, the proposed model showed a more balanced and superior performance across all classes, providing a more reliable framework for classification accuracy.

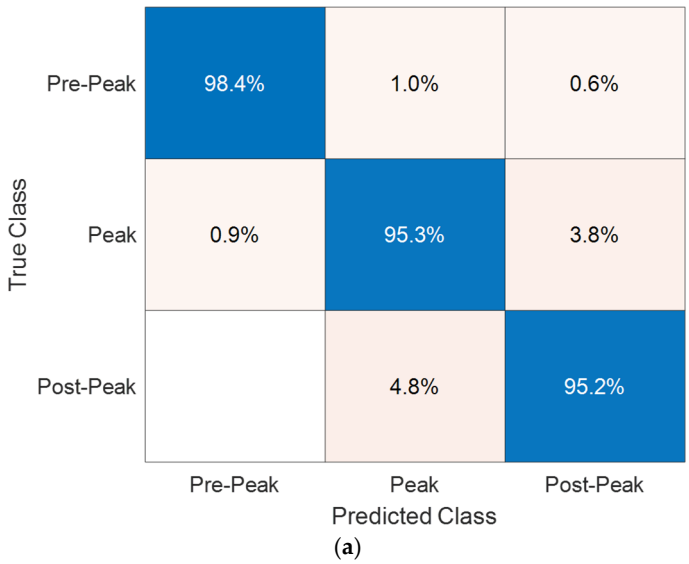



**Figure 10.** *Cont.*

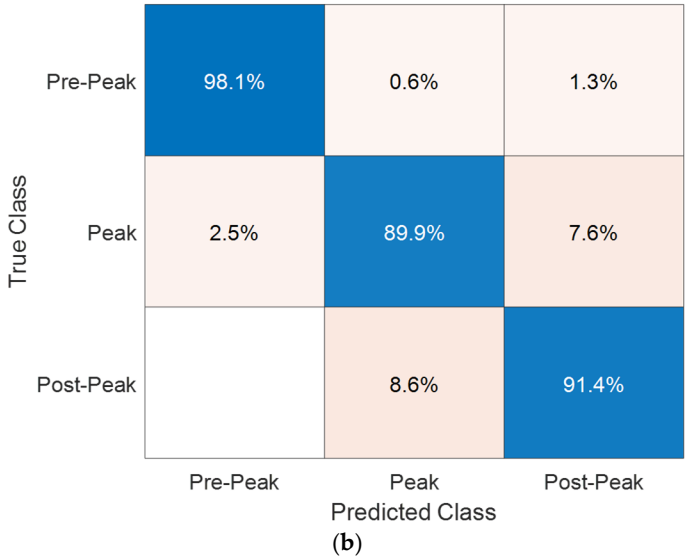



**Figure 10.** Confusion matrices showing the classification performance of (**a**) the proposed model and (**b**) the SVM-based model over the pre-peak, peak, and post-peak growth and development stages.

The proposed model and other developed models were comprehensively analyzed using several evaluation metrics, including precision, recall, and F1 score. The results of these evaluations are presented in Table 6. The results in Table 6 show that the proposed model effectively addresses nonlinear dynamics and consistently outperforms other models in all evaluation metrics used in this study. Although the performance metrics of the FFT-based model and the proposed model appear to be similar, it is important to note that the proposed model achieves this performance with a minimal number of selected features. This highlights the computational efficiency of the proposed model, making it superior to other models not only in terms of classification performance but also in terms of computational cost.

**Table 6.** Evaluation metrics for the proposed model and other developed models.

| **Model** | **FFT** | | | **Box Counting** | | | **Pre-Processed FFT** | | |
|---|---|---|---|---|---|---|---|---|---|
| | **Prec (%)** | **Rec (%)** | **F1 Score (%)** | **Prec (%)** | **Rec (%)** | **F1 Score (%)** | **Prec (%)** | **Rec (%)** | **F1 Score (%)** |
| kNN | 96.00 | 95.98 | 95.99 | 95.68 | 95.67 | 95.67 | 96.31 | 96.30 | 96.31 |
| SVM | 92.89 | 92.91 | 92.90 | 93.23 | 93.24 | 93.23 | 93.10 | 93.12 | 93.11 |

The classification results of the proposed model and the SVM-based model, using both the full feature set and the selected features, are presented in Table 7. The results indicate that the classification accuracy is higher for both models when using the selected features compared to the full feature set. Specifically, the proposed model achieved an accuracy of 96.30% with the selected features, compared to 94.18% with the full feature set. Similarly, the SVM-based model achieved an accuracy of 94.60% with the selected features, which dropped to 93.12% when using the full feature set. These results demonstrate that the selected features significantly improve the classification performance while reducing the computational cost. The proposed model outperformed the SVM-based model in both scenarios, highlighting its superior efficiency and accuracy. The feature selection process effectively eliminated redundant information, resulting in a more robust and computationally efficient model. The experimental results confirm that the proposed model can classify orthodontic growth stages with high accuracy and low computational cost.

This makes the model suitable for real-time applications, providing a practical and reliable solution for clinical use.

**Table 7.** Classification accuracy of the proposed model and the SVM-based model using the full feature set and selected features.

| Model | Selected Feature Acc | Full Feature Acc |
|---|---|---|
| kNN | 96.30 | 94.18 |
| SVM | 94.60 | 93.12 |

## 5. Conclusions and Future Directions

This study presents a novel framework that combines chaotic functional connectivity matrices, fractal dimension analysis, and advanced optimization techniques to classify orthodontic growth and development stages using lateral cephalometric radiographs. By addressing the inherent nonlinear dynamics of cervical vertebrae morphology, the proposed approach demonstrated its ability to achieve high classification accuracy and efficiency. The integration of fractal dimension analysis, using FFT, box counting, and pre-processed FFT methods, with chaotic maps provided a detailed representation of structural complexity and connectivity patterns. The results confirmed that these advanced techniques, when coupled with the metaheuristic PO algorithm and kNN classifier, provide a powerful solution for optimizing feature selection and reducing computational complexity without compromising performance. The proposed model significantly outperformed traditional diagnostic methods, such as hand–wrist radiographs, by providing a non-invasive, radiation-free, and automated assessment of skeletal maturation. By using wrapper-based feature selection, the model achieved a balance between accuracy and computational efficiency, making it suitable for real-time clinical applications. This study not only highlights the potential of AI-driven methods in orthodontics but also demonstrates how the synergy of chaotic maps, fractal dimensions, and functional connectivity matrices can transform the way growth stages are assessed. Building on these findings, future research could explore the following directions to further improve the applicability and performance of the framework:

i. Automated vertebra detection: The development of algorithms to automatically identify and crop C2, C3, and C4 vertebrae will streamline pre-processing and improve the efficiency of the model.
ii. Longitudinal studies: Conducting longitudinal studies to track skeletal growth patterns over time would provide deeper insights into the progression of orthodontic growth stages.
iii. Real-time clinical implementation: Optimizing the computational pipeline for real-time use through hardware acceleration or edge computing devices could facilitate seamless integration into orthodontic workflows.
iv. Multimodal data integration: Combining cephalometric radiographs with other imaging modalities, such as cone beam computed tomography, could provide a more complete understanding of skeletal maturation and growth patterns.

**Author Contributions:** Conceptualization, O.C. and A.A.; methodology, Y.B.Ö., A.A. and O.C.; software, Y.B.Ö. and A.A.; validation, Y.B.Ö., O.C. and A.A.; formal analysis, O.C., Y.B.Ö. and A.A.; investigation, A.A., O.C. and Y.B.Ö.; data curation, O.C., Y.B.Ö. and A.A.; writing—original draft preparation, Y.B.Ö., A.A. and O.C.; writing—review and editing, A.A. and O.C.; visualization, Y.B.Ö., A.A. and O.C.; supervision, O.C. and A.A. All authors have read and agreed to the published version of the manuscript.

**Funding:** This research received no external funding.

**Institutional Review Board Statement:** The study was conducted in accordance with the Declaration of Helsinki. Ethics committee approval for the study was given by the Non-Interventional Clinical Research Ethics Committee at Zonguldak Bulent Ecevit University study (decision no: 2024/15-5 and date: 4 September 2024).

**Informed Consent Statement:** Informed consent was obtained from all subjects involved in the study.

**Data Availability Statement:** The raw data supporting the conclusions of this article will be made available by the corresponding author on request.

**Conflicts of Interest:** The authors declare no conflicts of interest.

## References


1. Sarver, D.M. Interactions of hard tissues, soft tissues, and growth over time, and their impact on orthodontic diagnosis and treatment planning. *Am. J. Orthod. Dentofacial Orthop.* **2015**, *148*, 380–386. [CrossRef] [PubMed]
2. Buschang, P.H.; Roldan, S.I.; Tadlock, L.P. Guidelines for assessing the growth and development of orthodontic patients. *Semin. Orthod.* **2017**, *23*, 321–335. [CrossRef]
3. Lai, E.H.H.; Liu, J.P.; Chang, J.Z.C.; Tsai, S.J.; Yao, C.C.J.; Chen, M.H.; Chen, Y.J.; Lin, C.P. Radiographic assessment of skeletal maturation stages for orthodontic patients: Hand-wrist bones or cervical vertebrae? *J. Formos. Med. Assoc.* **2008**, *107*, 316–325. [CrossRef] [PubMed]
4. Baccetti, T.; Franchi, L.; McNamara, J.A., Jr. The cervical vertebral maturation (CVM) method for the assessment of optimal treatment timing in dentofacial orthopedics. *Semin. Orthod.* **2005**, *11*, 119–129. [CrossRef]
5. de Almeida-Neto, P.F.; de Medeiros, J.A.; Medeiros, R.M.V.; Baxter-Jones, A.; de Matos, D.G.; Aidar, F.J.; Dantas, P.M.S.; de Araújo Tinoco Cabral, B.G. Reliability of biological maturation analyses performed by equations predicting skeletal age and peak height velocity with hand and wrist X-ray results. *Am. J. Hum. Biol.* **2022**, *34*, e23775. [CrossRef] [PubMed]
6. Jaqueira, L.M.F.; Armond, M.C.; Pereira, L.J.; Alcântara, C.E.P.D.; Marques, L.S. Determining skeletal maturation stage using cervical vertebrae: Evaluation of three diagnostic methods. *Braz. Oral Res.* **2010**, *24*, 433–437. [CrossRef]
7. Flores-Mir, C.; Nebbe, B.; Major, P.W. Use of skeletal maturation based on hand-wrist radiographic analysis as a predictor of facial growth: A systematic review. *Angle Orthod.* **2004**, *74*, 118–124. [PubMed]
8. Eninanç, İ.; Büyükbayraktar, Z.Ç. Assessment of correlation between hand-wrist maturation and cervical vertebral maturation: A fractal analysis study. *BMC Oral Health* **2023**, *23*, 798. [CrossRef]
9. Xie, L.; Tang, W.; Izadikhah, I.; Zhao, Z.; Zhao, Y.; Li, H.; Yan, B. Development of a multi-stage model for intelligent and quantitative appraising of skeletal maturity using cervical vertebras cone-beam CT images of Chinese girls. *Int. J. Comput. Assist. Radiol. Surg.* **2022**, *17*, 761–773. [CrossRef] [PubMed]
10. Santiago, R.C.; de Miranda Costa, L.F.; Vitral, R.W.F.; Fraga, M.R.; Bolognese, A.M.; Maia, L.C. Cervical vertebral maturation as a biologic indicator of skeletal maturity: A systematic review. *Angle Orthod.* **2012**, *82*, 1123–1131. [CrossRef]
11. Pamukcu, U.; Ispir, N.G.; Akay, G.; Karadag Atas, O.; Gungor, K.; Toraman, M. Evaluation of the compatibility of C2, C3, and C4 fractal dimension values with hand-wrist and cervical vertebra maturation methods in determining skeletal maturation. *Dentomaxillofac. Radiol.* **2022**, *51*, 20220113. [CrossRef] [PubMed]
12. Kök, H.; Acilar, A.M.; İzgi, M.S. Usage and comparison of artificial intelligence algorithms for determination of growth and development by cervical vertebrae stages in orthodontics. *Prog. Orthod.* **2019**, *20*, 41. [CrossRef] [PubMed]
13. Radwan, M.T.; Sin, Ç.; Akkaya, N.; Vahdettin, L. Artificial intelligence-based algorithm for cervical vertebrae maturation stage assessment. *Orthod. Craniofac. Res.* **2023**, *26*, 349–355. [CrossRef]
14. Amasya, H.; Yildirim, D.; Aydogan, T.; Kemaloglu, N.; Orhan, K. Cervical vertebral maturation assessment on lateral cephalometric radiographs using artificial intelligence: Comparison of machine learning classifier models. *Dentomaxillofac. Radiol.* **2020**, *49*, 20190441. [CrossRef] [PubMed]
15. Makaremi, M.; Lacaule, C.; Mohammad-Djafari, A. Deep learning and artificial intelligence for the determination of the cervical vertebra maturation degree from lateral radiography. *Entropy* **2019**, *21*, 1222. [CrossRef]
16. Atici, S.F.; Ansari, R.; Allareddy, V.; Suhaym, O.; Cetin, A.E.; Elnagar, M.H. AggregateNet: A deep learning model for automated classification of cervical vertebrae maturation stages. *Orthod. Craniofac. Res.* **2023**, *26*, 111–117. [CrossRef]
17. Khazaei, M.; Mollabashi, V.; Khotanlou, H.; Farhadian, M. Automatic determination of pubertal growth spurts based on the cervical vertebral maturation staging using deep convolutional neural networks. *J. World Fed. Orthod.* **2023**, *12*, 56–63. [CrossRef]
18. Sebastián, M.V.; Navascués, M.A. A relation between fractal dimension and Fourier transform–electroencephalographic study using spectral and fractal parameters. *Int. J. Comput. Math.* **2008**, *85*, 657–665. [CrossRef]
19. Li, J.; Du, Q.; Sun, C. An improved box-counting method for image fractal dimension estimation. *Pattern Recognit.* **2009**, *42*, 2460–2469. [CrossRef]

20. Rakshe, C.; Kunneth, S.; Sundaram, S.; Murugappan, M.; Agastinose Ronickom, J.F. Autism spectrum disorder diagnosis using fractal and non-fractal-based functional connectivity analysis and machine learning methods. *Neural Comput. Appl.* **2024**, *36*, 12565–12585. [CrossRef]
21. Chen, L.; Liu, J.; Xu, T.; Long, X.; Lin, J. Quantitative skeletal evaluation based on cervical vertebral maturation: A longitudinal study of adolescents with normal occlusion. *Int. J. Oral Maxillofac. Surg.* **2010**, *39*, 653–659. [CrossRef]
22. Szemraj, A.; Wojtaszek-Słomińska, A.; Racka-Pilszak, B. Is the cervical vertebral maturation (CVM) method effective enough to replace the hand-wrist maturation (HWM) method in determining skeletal maturation?—A systematic review. *Eur. J. Radiol.* **2018**, *102*, 125–128. [CrossRef]
23. Fudalej, P.; Bollen, A.M. Effectiveness of the cervical vertebral maturation method to predict postpeak circumpubertal growth of craniofacial structures. *Am. J. Orthod. Dentofacial Orthop.* **2010**, *137*, 59–65. [CrossRef]
24. Kök, H.; Izgi, M.S.; Acilar, A.M. Determination of growth and development periods in orthodontics with artificial neural network. *Orthod. Craniofac. Res.* **2021**, *24*, 76–83. [CrossRef]
25. Atici, S.; Pan, H.; Elnagar, M.H.; Allareddy, V.; Suhaym, O.; Ansari, R.; Cetin, A.E. Classification of the cervical vertebrae maturation (CVM) stages using the Tripod network. In Proceedings of the IEEE International Conference on Acoustics, Speech and Signal Processing (ICASSP), Rhodes Island, Greece, 4–10 June 2023.
26. Kresnadhi, G.A.; Nurrajab, M.F.; Ilmi, A.Z.; Septiawan, M.A.; Handayani, A.; Adiprawita, W.; Anshori, I. Comparative analysis of ResNet101, InceptionV3, and InceptionResnetV2 architectures for cervical vertebrae maturation stage classification. In Proceedings of the International Conference on Electrical Engineering and Informatics (ICEEI), Bandung, Indonesia, 10–11 October 2023.
27. Motie, P.; Mohammad-Rahimi, H.; Hassanzadeh-Samani, S.; Razzaghi, N.; Behnaz, M.; Shahab, S.; Motamadian, S.R. Improving cervical maturation degree classification accuracy using a multi-stage deep learning approach. *Res. Sq.* **2024**. [CrossRef]
28. Li, H.; Li, H.; Yuan, L.; Liu, C.; Xiao, S.; Liu, Z.; Zhou, G.; Dong, T.; Ouyang, N.; Liu, L.; et al. The psc-CVM assessment system: A three-stage type system for CVM assessment based on deep learning. *BMC Oral Health* **2023**, *23*, 557. [CrossRef]
29. Akay, G.; Akcayol, M.A.; Özdem, K.; Güngör, K. Deep convolutional neural network—The evaluation of cervical vertebrae maturation. *Oral Radiol.* **2023**, *39*, 629–638. [CrossRef]
30. Benesty, J.; Chen, J.; Huang, Y.; Cohen, I. Pearson Correlation Coefficient. In *Noise Reduction in Speech Processing. Springer Topics in Signal Processing*; Springer: Berlin/Heidelberg, Germany, 2009; Volume 2, pp. 37–40.
31. Abdollahzadeh, B.; Khodadadi, N.; Barshandeh, S.; Trojovský, P.; Gharehchopogh, F.S.; El-kenawy, E.S.M.; Laith, A.; Mirjalili, S. Puma optimizer (PO): A novel metaheuristic optimization algorithm and its application in machine learning. *Clust. Comput.* **2024**, *27*, 5235–5283. [CrossRef]
32. Zhang, S.; Li, X.; Zong, M.; Zhu, X.; Wang, R. Efficient kNN classification with different numbers of nearest neighbors. *IEEE Trans. Neural Netw. Learn. Syst.* **2018**, *29*, 1774–1785. [CrossRef]
33. Zhang, S. Cost-sensitive KNN classification. *Neurocomputing* **2020**, *391*, 234–242. [CrossRef]
34. Sokolova, M.; Lapalme, G. A systematic analysis of performance measures for classification tasks. *Inf. Process Manag.* **2009**, *45*, 427–437. [CrossRef]


**Disclaimer/Publisher's Note:** The statements, opinions and data contained in all publications are solely those of the individual author(s) and contributor(s) and not of MDPI and/or the editor(s). MDPI and/or the editor(s) disclaim responsibility for any injury to people or property resulting from any ideas, methods, instructions or products referred to in the content.